

1
2
3
4
5
6
7
8
9
10
11
12
13
14
15
16
17
18
19
20
21
22
23
24
25
26
27
28
29
30
31
32
33
34
35
36
37
38
39
40
41
42
43
44
45
46
47
48
49
50
51
52
53
54
55
56
57
58
59
60

1 Lithological control on fracture cementation in the Keuper Marl
2 (Triassic), north Somerset, UK

3 **QINGFENG MENG[†], JOHN HOOKER & JOE CARTWRIGHT**

4 *Department of Earth Sciences, University of Oxford, South Parks Road, Oxford, OX1 3AN, UK*

5 [†] Author for correspondence: meng.qingfeng@hotmail.com

Abstract: The spatial arrangement of gypsum veins as preserved natural hydraulic fractures have been characterized in the Triassic Keuper Marl Formation (UK), a caprock for hydrocarbon reservoirs and CO₂ sequestration. The outcropping marls are subdivided into five discrete fracture units based on the presence and abundance of gypsum veins. The nodular gypsum in evaporite horizons provides excess gypsum for nodule-rooted horizontal gypsum veins. Our petrographic observations demonstrate that the development of gypsum veins in beds lacking macroscopic evaporites is closely associated with disseminated gypsum cement in the marls. We interpret that the gypsum veins in marl are sourced from disseminated gypsum cements in the host rocks, based on stratigraphic correlations, and much lower Sr concentrations than gypsum nodules. Gypsum was transported to adjacent veins mainly through diffusion in the low-permeability marls. The localization of gypsum veins, varied Sr concentrations of veins and nodules indicate that the diagenetic fluids are a mix of connate water with meteoric water rather than brines transported from evaporite beds along faults to non-evaporite beds. This results in the absence of gypsum fillings in fractures in rocks without primary gypsum cements. The study implies that the cementation of natural fractures in low-permeability rocks can highly depend on the presence of cement minerals in the host rock.

Key words: mudstone; fracture cementation; fracture stratigraphy; hydraulic fracture

1. Introduction

Mudrocks and evaporites are the most common caprock lithologies for hydrocarbon reservoirs worldwide because of their small pore sizes, low permeabilities, and ductile mechanical properties (Grunau, 1987). However, the sealing capacity of caprocks can be greatly reduced by fluid leakage through opening-mode fractures and faults (Ingram & Urai, 1999; Aydin, 2000;

Cartwright et al., 2007). Although fractures can reduce or block fluid flow after complete sealing (e.g. Laubach, 2003; Rustichelli et al., 2016; Hooker et al., 2017), sealed fractures as mineral veins are prone to reactivation and reopen due to the weak chemical bonds between cement and wall rocks (Gale & Holder, 2008, 2010). In mudrocks, fracture systems commonly exhibit a heterogeneous distribution, which can be described as discrete units in fracture stratigraphy with different rock compositions, textures diagenesis, and also the intrinsic tendency for fractures to remain open or to seal (Laubach et al., 2009; Gale et al., 2014). Understanding the fracture stratigraphy of caprock successions with a similar loading history has been increasingly viewed as a key component in assessing the sealing capacity of the caprocks (Ingram & Urai, 1999; Ogata et al., 2014; Laubach et al., 2009).

The Mercia Mudstone Group (MMG) consists of low-permeability marls and acts as a regional seal for the lower hydrocarbon reservoirs in the Sherwood Sandstone Group in the East Irish Sea and the Wessex Basin (Ruffell, 1990; Seedhouse & Racey, 1997). The Mercia Mudstone has also been considered as the caprock for carbon capture and storage sites in the Irish Sea Basin and the Southern North Sea Basin (Armitage et al., 2013, 2016; Williams et al., 2014). Previous studies have reported the occurrence of gypsum veins in the outcropping Mercia Mudstone in north Somerset, UK (Cosgrove, 2001; Philipp, 2008), which could serve as an ideal analogue for subsurface fracture prediction and reservoir modeling. However, the heterogeneous distribution of the gypsum veins and their controlling factors have received much less attention.

This paper reports the heterogeneous arrangement of gypsum veins in the Triassic Mercia Mudstone at outcrops in North Somerset, UK. The paper starts by describing the discrete fracture units and the mineral compositions of the marls in the Mercia Mudstone, then presents the geochemical characteristics of gypsum veins, nodules and fault-related veins. The aims of this

paper are (1) to examine the control of lithology on fracture and vein distribution in mudstone; (2) to investigate the mode of mass transport and fluid movement in low-permeability rocks; (3) to obtain a better understanding of the extent of hydraulic fractures and their heterogeneous distribution in mudstone and shale. This paper attempts to provide an analogue for fractured mudrocks exhibiting a high heterogeneity in distribution of fracture cementation.

2. Geological setting

2.a. Distribution and deposition of the Mercia Mudstone

The MMG ranges from Mid-Triassic (Anisian) to late Triassic (Rhaetian) in age and comprises predominantly argillaceous materials and evaporites (Howard et al., 2008). The bulk rock consists of featureless, unfossiliferous red marls, horizons of sulphate nodules, subordinate grey and green siltstones, and sporadic sandstones (Warrington, 1980; Whittaker & Green, 1983; Wilson, 1993). The MMG lies between the Lower Triassic Sherwood Sandstone and the latest Triassic Penarth group, with a diachronous base and a slightly disconformable contact with the Penarth Group (Warrington & Ivimey-Cook, 1992). The thickness of the MMG varies from almost zero meters at depositional margins to a maximum of 1350 m in basin centre areas (Benton et al., 2002). The outcrop of the MMG extends northward from Lyme Bay, through Somerset and South Wales, and continues northwards through much of the central Midlands (Hobbs et al., 2002; Howard et al., 2008). The outcrop bifurcates around the Pennine Anticline, with the western limb extending northward from Cheshire to the West Lancashire, and the Eastern limb spreading over East Midlands and Northeast England.

The MMG has been suggested to be deposited either in subaqueous inland hypersaline lakes or an inland sea (Warrington, 1974; Arthurton, 1980; Ruffell, 1991), or in giant playas or desert

plains (Tucker, 1977, 1978). The sediments were deposited on mudflats in four main ways (Arthurton, 1980; Warrington & Ivimey-Cook, 1992; Talbot et al., 1994), including (1) settling out of mud and silt in playa lakes; (2) rapid deposition of sheets of silts and sands by flash floods; (3) accumulation of wind-blown dust on surfaces of wet mudflats; and (4) chemical precipitation of gypsum and halite from hypersaline water bodies. The MMG underwent continued burial during the Triassic and Jurassic, reaching a maximum burial depth of 2.4 km, which is then followed by uplift during middle Cretaceous. The MMG can be subdivided into the lower Keuper Marl Formation and the upper Tea Green Marl Formation (or Blue Anchor Formation) (Whittaker & Green, 1983). The Keuper Marl mainly comprises undifferentiated red blocky marls, whilst the Tea Green Marl contains interbedded red, green or black marl and grey dolostone.

2.b. Mineral composition and diagenesis

Marl and siltstone dominate the facies of the Mercia Mudstone. The marls mainly comprise clay minerals, quartz, feldspar, carbonates, gypsum, halite, iron oxides, and other minor constituents (Arthurton, 1980; Bloodworth et al., 1993; Armitage et al., 2013).

The clay minerals are represented by a detrital phase of illite and chlorite, and an authigenic phase of mixed layer clays (generally chlorite-smectite), smectite, palygorskite and sepiolite (Hobbs et al., 2002). The authigenic clays have been suggested to form early in the diagenetic sequence by reactions between detrital clays and alkaline waters rich in Mg^{2+} (Leslie et al., 1993). Illite and chlorite have undergone transformation by the absorption of K^+ by illite and Mg^{2+} by chlorite. Smectite formed as a result of reactions between detrital, degraded illite and magnesium rich waters, calcium, hydrogen, carbonate and sulphate ions (Bloodworth et al., 1993). Chlorite

1
2
3
4
5
6
7
8
9
10
11
12
13
14
15
16
17
18
19
20
21
22
23
24
25
26
27
28
29
30
31
32
33
34
35
36
37
38
39
40
41
42
43
44
45
46
47
48
49
50
51
52
53
54
55
56
57
58
59
60

95 formed from magnesium rich smectite during burial when the temperature exceeded 100 °C and
96 sufficient aluminium ions were provided (Leslie et al., 1993).

97 Quartz is present throughout the marl as the dominant detrital non-clay fraction (Arthurton, 1980;
98 Hobbs et al., 2002). Quartz is usually sand to silt sized, and well to poorly sorted. The grain
99 shape varies between angular and sub-rounded. Quartz overgrowth often occurs, sometimes
100 resulting in welded grain contacts (Smith et al., 1974).

101 Calcite and dolomite are important components of the marl as the main cementing agents
102 (Armitage et al., 2013; Hobbs et al., 2002). Dolomite is often the dominant carbonate and could
103 comprises up to 50% of the carbonate-rich beds. Dolomite usually occurs as either as finely
104 disseminated particles or as euhedral rhombs. Calcite is often present as discrete patches. The
105 authigenic carbonates fill intergranular pore spaces, and significantly reduce the porosity and
106 permeability of the marl (Armitage et al., 2016).

107 Calcium sulphate is a minor component in the marl (Taylor, 1983; Wilson, 1990; Gallois, 2001;
108 Howard et al., 2008). It appears as both the hydrous form gypsum and the anhydrous form
109 anhydrite. Gypsum and anhydrite were primarily deposited as cements in the mud in the near
110 surface zone. The sedimentary fabrics were later disrupted by dehydration of gypsum when the
111 ambient temperature exceeds 42 °C during burial. Anhydrite readily transforms to gypsum in the
112 presence of water when the sediments were uplifted to the near-surface zone (Murray, 1964).
113 The transition is generally complete at a depth of 50-100 m. Gypsum is usually found as nodular
114 masses, finely disseminated crystals or vein fills.

115 Halite constitutes minor or trace components of the marl; however, it is usually not observed
116 within 40-60 m below the surface because of the high solubility (Howard et al., 2008; Hobbs et

al., 2002). Iron is present as Fe^{3+} in the red marls, whilst it appears in the reduced form of Fe^{2+} , usually pyrite, in the green or grey marls as a result of bacterial decomposition of organic matter (Leslie et al., 1993). Other non-clay minerals present as minor constituents include feldspar and heavy minerals (Old, 1991; Kellaway et al., 1993).

2.c. Local setting

The study area is located on Warren Bay in the Watchet area, Somerset (Figure 1). The coastal cliffs expose the Keuper Marl in the footwall of the Helwell Bay Fault, and the Lower Jurassic Blue Lias in the hanging wall. The outcrop of the Keuper Marl is transected by multiple normal faults, some of which have been reactivated with kinematic evidence for reverse reactivation (Dart et al., 1995; Glen et al., 2005). Sub-horizontal and steep fibrous gypsum veins are commonly present in the low-permeability marls (Cosgrove, 2001; Philipp, 2008; Trude et al., 2012). It has been suggested that many of the veins were generated as hydraulic fractures in response to the N-S tectonic compression during Alpine Orogeny (Cosgrove, 1995, 2001). Both hydraulic fractures and pre-existing, northward dipping tectonic fractures have been filled by gypsum and thus preserved (Cosgrove, 2001).

3. Methods

We used an integrated field, petrographic and geochemical method to characterize gypsum veins and their host rocks along the cliffs in the study area. Field observations mainly focus on stratigraphic arrangement of gypsum veins and fractures, the occurrence of evaporite beds, rock color and lithology. 56 representative samples of gypsum veins from bulk marls and faults, gypsum nodules and rocks from each units were collected for thin section and geochemical analysis.

1
2
3 139 56 thin sections of veins were cut normal to vein planes and also fibre plunge directions, so that
4
5
6 140 vein textures and vein-wall contacts could be revealed. We made optical observations of
7
8 141 gypsum veins and the host rocks in polarized light microscopy. A gypsum plate is inserted in the
9
10 142 optical path between the thin sections and the polarizing filter, in order to enhance contrast in
11
12 143 weakly birefringent gypsum (first order grey, yellow) and other minerals. Polished thin sections
13
14
15 144 were also examined using a FEI Quanta 650 FEG Scanning Electron Microscope (SEM). Rock
16
17 145 fabric and mineral composition analysis were conducted using energy dispersive X-ray
18
19 146 spectroscopy (EDS) that is attached to the SEM.
20
21

22
23 147 Elemental concentrations of three gypsum veins in marls, two veins in faults and two gypsum
24
25 148 nodules (38 samples) were measured using inductively coupled plasma mass spectrometry (ICP-
26
27 149 MS). The samples were dissolved in a mixture of hydrochloric, nitric, and hydrofluoric acids,
28
29 150 followed by diluting them in 2% nitric acid for measurement on the Elan ICP-MS at the
30
31 151 Department of Earth Sciences, University of Oxford. The measurement has a high precision to
32
33 152 $\pm < 0.01\%$. Nine samples were extracted from a 2.9 cm thick gypsum vein every 3.3 mm from one
34
35 153 wall to the other, and five samples from a 1.7 cm thick vein. By sampling chemical
36
37 154 concentrations across the veins we are able to combine those data with petrographic
38
39 155 interpretations of vein widening in order to reconstruct changes in the fluid chemistry during
40
41 156 vein widening and cementation. The concentrations of trace and minor elements were analyzed
42
43 157 in order to evaluate the origin and composition of diagenetic fluids. The strontium concentrations
44
45 158 were studied to determine brine paleosalinity (Kushnir, 1980, 1982; Kasprzyk, 2003) and hence
46
47 159 sources of vein gypsum.
48
49
50
51
52
53

54
55 160 We also estimated the contents of gypsum cement and gypsum veins in the marls of vein-
56
57 161 containing units by analyzing SEM images and high-resolution field photos. Box areas of $1 \mu\text{m}^2$
58
59
60

and 1 m² were randomly selected in a SEM image and field photo from each units respectively. The number of blue pixels in SEM images (white pixels in field photos) were documented using Photoshop software. The ratio of blue (white) versus all pixels represents the content of gypsum.

4. Fracture stratigraphy

Fracture stratigraphy subdivides stratified rock into discrete fracture units defined by properties, such as extent, intensity, or some other observed fracture attributes, i.e. the intrinsic types or patterns of cement (Laubach et al., 2009). The Keuper Marl along the cliffs in the study area is here divided into five fracture units, according to the occurrence and abundance of gypsum veins (Figure 2). Each unit is described regarding the spatial distribution and geometry of gypsum veins, occurrence of gypsum nodules, with correlations to their host rock types and mineral compositions.

4.a. Unit 1

Unit 1 lies at the base of the outcrop as the oldest unit of the outcropping rocks (Figure 3). Unit 1 contains an intra-formational pale grey-green sandstone body at the base. The sandstone body is 8 m long and 1.5 meters thick (Figure 3A). The beds are planar or current-ripple laminated. The sandstone body comprises gypsum cemented sandstone. The sands are medium-coarse grained and medium-well sorted. The sands exhibit point or linear contacts, with gypsum cementing intergranular pore spaces (Figure 3C). It has been suggested that the sandstone body probably formed as a brief episode of sand-filled fluvial channels (Hobbs et al., 2002). Dense gypsum veins, including sub-horizontal veins and steeply dipping veins, are present in the sandstone (Figure 3B). Gypsum veins are tightly clustered with a spacing of 1-2 cm. Steep veins, which

1
2
3 183 terminate at the sandstone-marl boundary, are confined within the sandstones. Gypsum veins
4
5
6 184 occupy 14.2% of the rock volume (Table 1).
7
8

9 185 Red gypsiferous marls with sub-planar bedding overlie the sandstone body. The marls are rather
10
11 186 homogeneous in lithology and consist of apparently structureless mudstone. The marls contain 1-
12
13 187 2 cm thick sub-horizontal gypsum veins that closely conform to bedding. Vertical spacing of the
14
15
16 188 veins is 80 cm. Multiple nodular gypsum horizons, which are closely spaced, are observed within
17
18 189 the central intervals of the unit. The ratio of gypsum vein-volume to bulk rock volume is
19
20
21 190 approximately 7.1% (Table 1).
22
23

24 191 The marls mainly contain clay minerals as the matrix. Silt-sized quartz, albite and K-feldspar
25
26 192 grains are distributed throughout the marl and are supported by the clay matrix (Figure 3D).
27
28
29 193 Fine-grained dolomite occurs as discrete patches filling pore spaces. Gypsum, both in the form of
30
31 194 isolated needle-like elongate laths and crystal aggregates with indistinct boundaries and irregular
32
33
34 195 shapes, is present in the marls and accounts for 8.7% in volume.
35
36

37 196 **4.b. Unit 2**

38
39

40 197 Unit 2 is a 10.5 m thick interval comprising red, grey and green, highly gypsiferous silty marl
41
42 198 (Figure 4), which is separated from Unit 1 by a 6 cm thick gypsum vein. Two groups of nodular
43
44
45 199 gypsum horizons, each containing 4-5 horizons (Figure 4B), occur in this unit. The nodules vary
46
47 200 from several centimeters to 2 m in the horizontal dimension, and centimeters to 0.5 m in
48
49
50 201 thickness. Sub-horizontal veins and steep veins are intensively developed in this unit, with a
51
52 202 spacing of less than one decimeter. In the siltstone intervals, the rocks are highly damaged, with
53
54
55 203 the fractures filled with gypsum. The veins exhibit near-random orientations and a high
56
57 204 connectivity. Vein intensity is significantly higher in siltstones than in the red marls. Vein
58
59
60

spacing is commonly around 5 cm or less. The volume of gypsum veins takes up 25.4% of the total rock volume (Table 1). Interestingly, gypsum veins are much less abundant in the nodular gypsum horizons, especially the horizons between neighboring nodular horizons (Figure 4B).

The rocks exhibit a variety of fabrics ranging from finely laminated to approximately structureless. Fine siltstones and clay-bearing siltstones in grey, green colors occur at intervals throughout the unit (Figure 4C). The red marls comprise clay minerals, quartz, gypsum and dolomite (Figure 4D). The quartz grains are mainly fine-grained and occur either as discrete patches or in closely packed clusters. Overgrowth of quartz is commonly observed, which results in boundary welding of quartz cements. Unit 2 contains a high content (28.2%) of gypsum. Gypsum appears either as pore-filling linear laths or as poikilotopic cements encasing quartz (both detrital grains and cements), dolomite and less commonly clay minerals.

4.c. Unit 3

Unit 3 is characterized by massive red calcareous marls, with planar bedding which is marked by the green marl beds (Figure 5A-C). Four groups of nodular horizons occur in this unit (Figure 5B). The lowest group of nodular gypsum horizons is here defined as the boundary of Units 2 and 3. The normal faults, which transects the outcrop, are commonly observed to be cemented with gypsum only in the segments adjacent to nodular horizons. In contrast to Unit 2, gypsum veins are not developed in the bulk rock of the nodule-free horizons. The marls are highly fractured, with a horizontal fracture spacing of approximately 0.4 m. Many steep opening-mode fractures, including those adjacent to nodular horizons, are exposed in the cliffs and exhibit no signs of cementation by gypsum (Figure 5C).

226 The rocks contain clay minerals, quartz, albite, K-feldspar, calcite and dolomite (Figure 5D).
227 Gypsum is totally absent in the non-evaporite beds. The silt grains of quartz, albite and K-
228 feldspar are poorly sorted and angular. Pore spaces are cemented by calcite and dolomite, with
229 little porosity preserved. Dolomite is commonly present as euhedral rhombs.

230 **4.d. Unit 4**

231 Unit 4 resembles Unit 1 regarding the lithology. This unit is represented by red marls (Figure
232 6A-B), and can be distinguished from the Unit 3 by a 10 cm thick green siltstone bed and a group
233 of nodular horizons underlying the green bed. Nine nodular gypsum horizons occur in Unit 4.
234 However, gypsum veins are more abundant in the intervals between nodules. Sub-horizontal
235 veins and NW-SE striking, north dipping veins exhibit a high intensity and connectivity (Figure
236 6B). The intensively developed vein network in Unit 4 exhibits a sharp contrast with both the
237 underlying Unit 3 and the overlying Unit 5. Vein spacing is commonly less than 10 cm. Gypsum
238 veins represent 10.3% of the total rock volume (Table 1). The length and height of single veins is
239 often difficult to determine due to the frequent linkage with neighboring veins. The steep veins
240 terminate abruptly at the level of the topmost nodular gypsum horizon, which bounds Unit 4 and
241 Unit 5.

242 The marls consist of clays, quartz, albite, K-feldspar, dolomite and gypsum (Figure 6C). This
243 unit also contains three green siltstone beds. Silt-sized quartz, albite and K-feldspar are sparsely
244 scattered in the rock matrix of marls, with an average spacing of 30 μm . Fine-grained dolomite
245 fills the pore spaces as the intergranular cements. Gypsum laths, either as discrete individuals or
246 closely packed aggregates, cement the marls, occupying 9.5% of the rock volume (Table 1).

247 **4.e. Unit 5**

248 This unit is present as homogeneous red marls (Figure 6A-B). Unit 5 and Unit 4 are bounded by
249 a nodular horizon and a laterally impersistent siltstone bed. The striking feature of Unit 5 is the
250 absence of both gypsum nodules and veins. Interestingly, this unit is transected by many NW-SE
251 striking, north dipping fractures that are aligned parallel to the steep veins in Unit 4 (Figure 6B).
252 These fractures are entirely unmineralised.

253 The marls comprise clays, quartz, albite, calcite and dolomite (Figure 6D). Gypsum is not found.
254 Quartz and albite are very fine grained. Calcite and dolomite act as the only pore cements.
255 However, apparent pore spaces in varied sizes are commonly observed.

256 In summary, within Units 1 and 4 gypsum veins only occur in the nodular-free intervals, which
257 both contain gypsum cement in the host rock. Nodular gypsum horizons are present in all units
258 except Unit 5. Gypsum veins are mainly concentrated in the nodular horizons that lack gypsum
259 in the host rock. Apparent pore space is only present in Unit 5.

260 **5. Nodule-rooted gypsum veins**

261 In Units 1-4, gypsum veins occur in nodular gypsum horizons, which link neighboring gypsum
262 nodules (Figure 7). This feature has also been reported by Philipp (2008). The vein orientations
263 are mainly sub-horizontal and parallel to the long axes of the nodules. The veins do not cross-cut
264 the nodules; instead the veins are rooted in the nodules. Nodule-rooted veins propagated laterally
265 and often coalesced with adjacent veins or nodules, or pinched out in the host rock.

266 **6. Gypsum in the host rock**

267 The distribution of gypsum veins in nodule-free intervals is positively correlated with the
268 presence of gypsum crystals in the host rocks. In clay-rich marls, gypsum is commonly present

1
2
3 269 as sand-sized laths, exhibiting near random orientations (Figure 8A). Many sub-parallel gypsum
4
5 270 laths are accumulated as aggregates, appearing as blocky gypsum masses. In highly gypsiferous
6
7
8 271 marls, the laths exhibit a high density and connectivity. The original texture seems to be
9
10 272 interrupted during diagenesis, as represented by the rotation of the laths. This results in the
11
12 273 parallel alignment of the crystals, exhibiting a clear texture. In coarser-grained rocks, including
13
14 274 silty marls, clay-rich siltstones and siltstones, gypsum is more diffusely disseminated within the
15
16
17 275 rocks (Figure 8B). Gypsum exhibits blocky textures and indistinct boundaries, forming
18
19 276 poikilotopic cements that support all other grains, including early-formed pore cement of
20
21 277 dolomite.
22
23
24

25
26 278 Crystal aggregates of gypsum laths are commonly present in clay-rich marls around gypsum
27
28 279 veins (Figure 8C). The gypsum laths are typically closely arranged and exhibit a preferred
29
30 280 orientation sub-parallel to vein walls. In silty marls, gypsum mainly appears as lenticular blocky
31
32 281 masses in the rocks adjacent to gypsum veins. In siltstones gypsum is widely disseminated
33
34 282 around gypsum veins. This results in indistinct boundaries of gypsum veins which can be
35
36 283 difficult to distinguish from the enclosing gypsum. EDS data demonstrate that gypsum in the
37
38 284 wall rock of gypsum veins is commonly attached to vein walls, exhibiting direct contacts with
39
40 285 the faces of gypsum crystals in veins (Figure 8D).
41
42
43
44

45
46 286 Many minor veins are commonly observed in gypsiferous marl, linking larger veins with blocky
47
48 287 gypsum masses in the adjacent areas (Figure 8E-H). The minor veins are often aligned at high
49
50 288 angles to the large veins. Fibres in the minor veins are approximately normal to vein walls
51
52 289 (Figure 8E-F, 8H). The minor veins are rooted either in the larger veins or in the blocky gypsum
53
54 290 masses, with the maximum aperture in the node points and a tapering tip propagating towards the
55
56 291 neighboring gypsum bodies (Figure 8H). It is interpreted that those minor veins formed as
57
58
59
60

tension gashes during lateral propagation of the large veins. The linkage of veins and gypsum masses often leads to segmentation of the enclosed host rock into multiple segments of varied sizes (Figure 8G-H).

7. Elemental concentration

The co-precipitation of minor and trace elements into CaSO_4 acts as a function of temperature, brine concentration and growth rate (Kushnir, 1980). Hence, elemental concentrations in gypsum has been extensively studied to evaluate paleosalinity, the depositional environment, brine origin and diagenetic evolution of the sediments (e.g. Lu et al., 1997, 2002; Kushnir, 1980, 1982; Kasprzyk, 2003; Machel, 1985). The geochemical measurements reveal that the gypsum nodules and veins are very pure, and many trace elements are below the detection limits (Supplementary Table S1). The concentrations of Na, Mg and Sr, as the commonly studied elements as indicators for paleoenvironment and paleosalinity (Kushnir, 1980; Lu et al., 1997; 2002), are plotted in figure 9 for nodules, veins (in marl) and fault-related veins. The concentrations of Na and Mg in the three types of gypsum largely overlap. The higher concentration of Na (67 ppm) and Mg (19 ppm) from a gypsum vein sample compared to all other samples (Na < 23 ppm, Mg < 12 ppm) is possibly influenced by fluid or solid inclusions within the vein.

Strontium incorporates into the gypsum lattice mainly by substitution of Ca^{2+} (Ichikuni and Musha, 1978). The equilibrium partition coefficient of strontium increases when the brine concentration rises, hence strontium concentration has revealed itself as the most useful as a paleosalinity indicator (Kushnir, 1980; Rosell et al., 1998). Both primary and secondary gypsum can be characterized by their strontium content (Rosell et al., 1998; Lu et al., 2002; Playà et al.,

2000; Leslie et al., 1997). Sr is the sole minor constituent in the structure of gypsum in our samples. The concentrations of Sr of gypsum veins in the bulk marls and faults are similar and generally undifferentiable. Importantly, the Sr concentrations from gypsum nodules are one order of magnitude greater than those from the gypsum veins in marls and the fault-related veins (Figure 9). Such high Sr concentrations in nodules have been suggested to be induced by evaporation in brine lakes during primary deposition of sulphate (Attendorn & Bowen, 1997), and further validate the idea that the nodular gypsum horizons in the Keuper Marl represent the stages of basin drying (Cosgrove, 2001).

Single gypsum vein samples are pure in composition and exhibit rather consistent elemental concentrations from one wall to the other (Figure 10). Sr concentrations are clustered around 150 ppm. This indicates a rather constant brine concentration during precipitation of vein gypsum.

8. Discussion

Based on our field and petrographic observations of gypsum veins, elemental analysis of gypsum veins, nodules and fault veins, the discussion mainly focuses on questions regarding the source of vein gypsum, the hydraulic system, and the mass transport mode in the low-permeability marls.

8.a. Source of vein gypsum

The formation of gypsum vein networks in the marls of Units 1, 2 and 4 would be expected to require vast quantities of gypsiferous solutions for vein-filling due to the low solubility of gypsum (Shearman et al., 1972). A common feature of those veins is that they are predominantly concentrated in non-nodular intervals.

The presence of gypsum veins in non-nodular beds has been reported in previous studies (Shearman et al., 1972; Gustavson et al., 1994; Mohamed El Tabakh & Warren, 1998; Cosgrove, 2001; Rustichelli et al., 2016). Gypsum-filling of fractures has been largely attributed to externally sourced gypsum (Shearman et al., 1972; Machel, 1985; Gustavson et al., 1994). It has been suggested that the excess gypsum, produced during anhydrite-gypsum transition, could have been delivered from more deeply buried dissolving evaporite beds to adjacent non-evaporite beds (Shearman et al., 1972; Philipp, 2008). Gypsum-rich fluids could then be focused into high-permeability pathways of tensile fractures in the mudstone. Those fractures could be simultaneously generated by the injection of gypsum-rich fluids (Shearman et al., 1972; Philipp, 2008) or have formed as pre-existing fractures that facilitated high salinity fluids entering the adjacent non-evaporite beds (Gustavson et al., 1994). Gypsum from an external source could then precipitate in those fractures and cause the final sealing of them. However, this hypothesis lacks supporting evidence from vein host rocks.

Our observations demonstrate that sub-horizontal gypsum veins are commonly present in all nodule-bearing units and link neighboring nodules (Figure 7). Those veins are interpreted to be sourced by their host nodules during anhydrite hydration (Figure 11). Nodule-rooted fractures, which could result from tensile stress concentration at the lateral margins of nodules (Philipp, 2008), were filled with excess gypsum derived from nodules. Crystallization pressure of gypsum, up to 15 MPa (Keulen et al., 2001), could lead to host rock rupturing and fracture propagation. An external source for gypsum in non-nodular beds is considered unlikely due to the following reasons:

- (1) Abundant non-filled fractures are present in non-evaporite horizons adjacent nodular horizons in Unit 3 (Figure 5C). This suggests that those fractures were not produced by

brecciating of the surrounding rocks by anhydrite-gypsum transition, and the nodular gypsum did not necessarily provide gypsum sources for fractures in adjacent beds.

(2) It is difficult to explain why fractures in Unit 5 are not filled, whereas Unit 4 contains dense veins (Figure 6A-B), if it was to be assumed that gypsum-rich fluids were advectively transported into these beds.

(3) The much lower (approximate one order of magnitude) Sr concentrations of gypsum veins than gypsum nodules (Figure 9) indicate that the nodules are possibly not the nutrient source for veins. This is because Sr is not appreciably fractionated by sulfate crystallization (Mohamed El Tabakh and Warren, 1998).

Given the fact that gypsum cement, either in the form of elongate laths or diffusely disseminated blocky gypsum, co-exists with gypsum veins in non-nodular beds, it is instead proposed that the local gypsum cement could have provided the source of calcium sulphate for the filling of adjacent veins. This idea is also evident from the contents of gypsum cement and gypsum veins in the host rock (Table 1), where a higher content of gypsum cement in the host rock corresponds to a higher content of gypsum veins. In this case, fractures could be filled by locally derived gypsum only in the bulk rocks containing gypsum cements. This is especially clear in Units 3 and 5, which lack gypsum veins and cements but contain abundant non-filled fractures (Figures 5C, 6B).

Based on the evidence above, the local source of gypsum is argued to be responsible for the filling of adjacent fractures as a result of redistribution of gypsum already present in the rock (Figure 11).

8.b. Hydraulic fracturing

The heterogeneous distribution of veins in the rather homogeneous Keuper Marl suggests that the diagenetic fluids are unlikely to be circulated from underlying evaporite beds for two main reasons:

(1) Gypsum veins are absent in Units 3 and 5, but are abundant in all other units. If the diagenetic fluids were from underlying evaporites, then surely the veins would be expected to exhibit a more homogeneous distribution in all fracture units. If the barren fractures in the Units 3 and 5 formed later than the gypsum veins, it is expected that such fractures would also occur in Unit 4 and could cross-cut the gypsum veins. However, all fractures in Unit 2 are filled with gypsum, indicating that fracture cementation postdates the formation of the barren fractures. Hence, the barren fractures, especially those parallel-aligned fractures in Unit 5, are interpreted to predate fracture cementation in vein-bearing units.

(2) Local faults, which penetrate into the fracture units without gypsum veins, only contain filling of gypsum in the segments adjacent to nodular horizons (Figure 5A-C). This observation does not favour a long distance brine migration along faults, and hence does not support the idea (Philipp, 2008) that faults acted as the main fluid migration paths.

The stratigraphic arrangement of gypsum veins, i.e. localized in Units 1, 2 and 4, indicates that the diagenetic fluids are more likely to be a mix of connate and meteoric waters. The input of low-salinity meteoric waters could also contribute to the decrease in the partition coefficient of strontium, and result in the relative low concentrations of Sr in vein gypsum. When the sediments were uplifted to shallow depths of the telogenetic zone, the marls would have come in

contact with low salinity, low temperature waters. Meteoric water is highly undersaturated with gypsum or anhydrite and will readily dissolve those calcium sulphates (Dronkert, 1987). This would result in anhydrite dissolution. However, not all sulphates have been dissolved because of the slow dissolution kinetics.

A pervasive increase in fluid pressure in the marl reacted as a response to the tectonic compression that facilitated the formation of hydraulic fractures and subsequent generation of veinlets (Cosgrove, 1995, 2001). The newly formed hydraulic fractures are considered as internal hydraulic fractures rather than intrusion hydraulic fractures (Engelder and Lacazette, 1990; Mandl, 2005, p27). Otherwise, it would be necessary to invoke a selective penetration of gypsum-rich brines into certain units and to completely bypass other units. The internal hydraulic fractures mainly include sub-horizontal bedding-parallel fractures which took advantage of bedding fissures with low tensile strengths (Shearman et al., 1972), and also bedding planes that diverted propagation of opening mode fractures (Gale et al., 2014; Lee et al., 2015). The pre-existing fractures, such as the north dipping, steep fractures, were reactivated and also filled with secondary gypsum.

8.c. Mass transport

In clay-rich rocks with a low permeability, which contains more prevalent fibrous mineral veins than other rock types (Cobbold et al., 2013), diffusion has been considered as the dominant mass-transport mechanism (Wiltschko & Morse, 2001; Lander & Laubach, 2015). Although diffusion is only effective within a small scale (<m) in rocks (Bickle & McKenzie, 1987), diffusion could produce fibrous veins with an aperture up to 10 cm (Fisher et al., 1995), accompanied with the depletion of the vein-forming elements in the surrounding rocks. For

1
2
3 423 gypsum veins in the low-permeability Keuper Marl, we argue that the mass transport from sites
4
5 424 of material source to gypsum veins occurred via a combined local advection during hydraulic
6
7 425 fracturing, and diffusion after the initial stage of fracture propagation. When hydraulic fractures
8
9 426 were opened against the least principle stress by fluid injection, advective fluids were sucked
10
11 427 into the fractures due to the pressure difference between the fracture and the wallrock. This could
12
13 428 have led to a much more effective mass transfer due to the high permeability the fractures
14
15 429 provide (Oliver & Bons, 2001; Laubach et al., 2004).
16
17
18
19

20
21 430 However, upon fracturing a rapid drop of pressure and pressure-dependent mineral solubility
22
23 431 would occur (Phillips, 1972; Henderson & McCaig, 1996), leading to precipitation of gypsum on
24
25 432 fracture walls and a final complete fracture sealing. The sealing of fractures eliminates the
26
27 433 chance of long distance mass transfer; however, the pressure difference between the host rock
28
29 434 and a thin fluid film vein-wall interfaces could lead to gypsum transported to adjacent vein walls
30
31 435 diffusively (Putnis et al., 1995; Bons et al., 2012). The lack of crack-seal textures in the gypsum
32
33 436 veins suggest that those veins grew incrementally without repeated re-opening events (Bons,
34
35 437 2000). The constant elemental concentrations in single gypsum veins suggest that the vein-filling
36
37 438 gypsum was possibly derived from a uniform source. This source is constrained to be the local
38
39 439 gypsum cement in adjacent rocks (Figure 11). This is evident from the concentration of
40
41 440 disseminated gypsum in the wallrocks and also its direct contacts with vein gypsum. The primary
42
43 441 rock fabrics have been modified by the diagenesis and redistribution of gypsum as expressed by
44
45 442 the distortion and accumulation of gypsum crystals, towards stability within the ambient
46
47 443 temperature and pressure regime (Dronkert, 1987). The transport distance is very low,
48
49 444 presumably at decimeter scale. This is evident from the rocks adjacent to the boundary of Units 4
50
51 445 and 5, of which the lower unit contains widespread gypsum whereas the upper units contain
52
53
54
55
56
57
58
59
60

1
2
3
4
5
6
7
8
9
10
11
12
13
14
15
16
17
18
19
20
21
22
23
24
25
26
27
28
29
30
31
32
33
34
35
36
37
38
39
40
41
42
43
44
45
46
47
48
49
50
51
52
53
54
55
56
57
58
59
60

gypsum in neither the fractures nor the rock matrix. A dominance of diffusion rather than advection could then be expected to account for mass transport.

In summary, the mass transport of gypsum is mainly through fluid advection during hydraulic fracturing, whilst veins derived their gypsum mainly by diffusion after the initial fracture propagation.

9. Conclusions

(1) The outcropping Keuper Marl in the Watchet area is subdivided into five fracture units. Disseminated gypsum as cement in the rocks is observed to co-exist with the development of gypsum veins in non-nodular beds.

(2) Gypsum veins in marls and faults exhibit much lower Sr concentrations than those from gypsum nodules.

(3) The nodule-rooted horizontal gypsum veins are sourced by excess gypsum from nodules in the evaporite beds. Differently, the gypsum veins in non-nodular beds derived nutrients from local gypsum cements in the surrounding host rocks.

(4) The sub-horizontal veins in non-nodular beds formed as hydraulic fractures. The diagenetic fluid is a mix of connate water and meteoric water rather than brines from nodular horizons.

(5) Gypsum was transported to walls of adjacent sealed gypsum veins through diffusion over a short distance, and was rarely transported to beds containing no depositional gypsum, leaving fractures in those beds unfilled.

(6) This study implies that fracture cementation by minerals in low-permeability rocks can highly depend on the presence of the same phase in the host rock.

Acknowledgements

This research is funded by Shell International Exploration and Production B.V. We thank Jon Wells for sample preparation and Owen Green for assistance with microscope imaging. Alex Dickson is thanked for assistance with geochemical measurements. We appreciate the editorial handling of this paper by Olivier Lacombe. Reviews by two anonymous reviewers significantly improved the quality of this paper.

References

- ARMITAGE, P., WORDEN, R., FAULKNER, D., APLIN, A., BUTCHER, A. & ESPIE, A. 2013. Mercia Mudstone Formation caprock to carbon capture and storage sites: petrology and petrophysical characteristics. *Journal of the Geological Society* **170**, 119-132.
- ARMITAGE, P., WORDEN, R., FAULKNER, D., BUTCHER, A. & ESPIE, A. 2016. Permeability of the Mercia Mudstone: suitability as caprock to carbon capture and storage sites. *Geofluids* **16**, 26-42.
- ARTHURTON, R. S. 1980. Rhythmic sedimentary sequences in the Triassic Keuper Marl (Mercia Mudstone Group) of Cheshire, northwest England. *Geological Journal* **15**, 43-58.
- ATTENDORN, H. G., BOWEN, R. 1997. *Radioactive and stable isotope geology*. Springer Science & Business Media, Berlin.

- 486 AYDIN, A. 2000. Fractures, faults, and hydrocarbon entrapment, migration and flow. *Marine*
487 *and petroleum geology* **17**, 797-814.
- 488 BEAR, J. 1972. *Dynamics of fluids in porous media*. American Elsevier, New York.
- 489 BENTON, M. J., COOK, E. & TURNER, P. 2002. *Permian and Triassic red beds and the*
490 *Penarth Group of Great Britain*. Joint Nature Conservation Committee.
- 491 BCIKLE, M. & MCKENZIE, D. 1987. The transport of heat and matter by fluids during
492 metamorphism. *Contributions to Mineralogy and Petrology* **95**, 384-392.
- 493 BLOODWORTH, A. & B. G. S. MINERALOGY GROUP. 1993. Clay mineral stratigraphy of
494 the Mercia Mudstone Group in the Nottingham area. Research report WG/93/29. British
495 Geological Survey, Keyworth.
- 496 BONS, P. D. 2000. The formation of veins and their microstructures. *Journal of the Virtual*
497 *Explorer* **2**, 12.
- 498 BONS, P. D., ELBURG, M. A. & GOMEZ-RIVAS, E. 2012. A review of the formation of
499 tectonic veins and their microstructures. *Journal of Structural Geology* **43**, 33-62.
- 500 CARTWRIGHT, J., HUUSE, M. & APLIN, A. 2007. Seal bypass systems. *AAPG Bulletin* **91**,
501 1141-1166.
- 502 COBBOLD, P. R., ZANELLA, A., RODRIGUES, N. & LOSETH, H. 2013. Bedding-parallel
503 fibrous veins (beef and cone-in-cone): worldwide occurrence and possible significance
504 in terms of fluid overpressure, hydrocarbon generation and mineralization. *Marine and*
505 *Petroleum Geology* **43**, 1-20.
- 506 COSGROVE, J. 1995. The expression of hydraulic fracturing in rocks and sediments. *Geological*
507 *Society, London, Special Publications* **92**, 187-196.

- 1
2
3 508 COSGROVE, J. 2001. Hydraulic fracturing during the formation and deformation of a basin: A
4
5 509 factor in the dewatering of low-permeability sediments. *AAPG Bulletin* **85**, 737-748.
6
7
8 510 DART, C. J., MCCLAY, K. & HOLLINGS, P. N. 1995. 3D analysis of inverted extensional
9
10 511 fault systems, southern Bristol Channel basin, UK. *Geological Society, London, Special*
11
12 512 *Publications* **88**, 393-413.
13
14
15 513 DRONKERT, H. 1987. Diagenesis of Triassic evaporites in northern Switzerland. *Eclogae*
16
17 514 *Geologicae Helvetiae* **80**, 397-413.
18
19
20 515 ENGELDER, T. & LACAZETTE, A. 1990. Natural hydraulic fracturing. In BARTON, C., &
21
22 516 STEPHANSSON, O. (Eds), *Rock joints*, Rotterdam, 35-43.
23
24
25 517 FISHER, D. M., BRANTLEY, S. L., EVERETT, M. & DZVONIK, J. 1995. Cyclic fluid flow
26
27 518 through a regionally extensive fracture network within the Kodiak accretionary prism.
28
29 519 *Journal of Geophysical Research: Solid Earth* **100**, 12881-12894.
30
31
32 520 GALE, J. F. & HOLDER, J. 2008. Natural fractures in the Barnett Shale: Constraints on spatial
33
34 521 organization and tensile strength with implications for hydraulic fracture treatment in
35
36 522 shale-gas reservoirs, The 42nd US Rock Mechanics Symposium (USRMS). American
37
38 523 Rock Mechanics Association.
39
40
41 524 GALE, J. F. & HOLDER, J. 2010. Natural fractures in some US shales and their importance for
42
43 525 gas production, *Geological Society, London, Petroleum Geology Conference Series*.
44
45 526 Geological Society of London **7**, 1131-1140.
46
47
48 527 GALE, J. F., LAUBACH, S. E., OLSON, J. E., EICHHUBL, P. & FALL, A. 2014. Natural
49
50 528 fractures in shale: A review and new observations. *AAPG Bulletin* **98**, 2165-2216.
51
52
53
54
55
56
57
58
59
60

- 529 GALLOIS, R. 2001. The lithostratigraphy of the Mercia Mudstone Group (mid-late Triassic) of
530 the south Devon coast. *Geoscience in south-west England. Proceedings of the Ussher*
531 *Society* **10**, 195-204.
- 532 GLEN, R., HANCOCK, P. & WHITTAKER, A. 2005. Basin inversion by distributed
533 deformation: the southern margin of the Bristol Channel Basin, England. *Journal of*
534 *Structural Geology* **27**, 2113-2134.
- 535 GRUNAU, H. R. 1987. A worldwide look at the cap-rock problem. *Journal of Petroleum*
536 *Geology* **10**, 245-265.
- 537 GUSTAVSON, T. C., HOVORKA, S. D. & DUTTON, A. R. 1994. Origin of satin spar veins in
538 evaporite basins. *Journal of Sedimentary Research* **64**, 88-94.
- 539 HENDERSON, I. & MCCAIG, A. 1996. Fluid pressure and salinity variations in shear zone-
540 related veins, central Pyrenees, France: implications for the fault-valve model.
541 *Tectonophysics* **262**, 321-348.
- 542 HOBBS, P., HALLAM, J., FORSTER, A., ENTWISLE, D., JONES, L., CRIPPS, A.,
543 NORTHMORE, K., SELF, S. & MEAKIN, J. 2002. Engineering geology of British
544 rocks and soils: Mudstones of the Mercia Mudstone Group. Research report RR/01/002,
545 British Geological Survey, Keyworth.
- 546 HOWARD, A., WARRINGTON, G., AMBROSE, K. & REES, J. 2008. A formational
547 framework for the Mercia Mudstone Group (Triassic) of England and Wales. Research
548 report RR/08/004, British Geological Survey, Keyworth.
- 549 HOOKER, J. N., CARTWRIGHT, J., STEPEHNSON, B., SILVER, C. R. P., DICKSON, A. J.
550 & HSIEH, Y. 2016. Fluid evolution in fracturing black shales, Appalachian Basin.
551 *AAPG Bulletin*, doi: 10.1306/10031616030.

- 552 ICHIKUNI, M. & MUSHI, S. 1978. Partition of strontium between gypsum and solution.
553 Chemical Geology **21**, 359-363.
- 554 INGRAM, G. M. & URAI, J. L. 1999. Top-seal leakage through faults and fractures: the role of
555 mudrock properties. *Geological Society, London, Special Publications* **158**, 125-135.
- 556 KASPRZYK, A. 2003. Sedimentological and diagenetic patterns of anhydrite deposits in the
557 Badenian evaporite basin of the Carpathian Foredeep, southern Poland. *Sedimentary*
558 *Geology* **158**, 167-194.
- 559 KELLAWAY, G., WELCH, F. B. A. & IVIMEY-COOK, H. 1993. *Geology of the Bristol*
560 *district: memoir for 1: 63 360 geological special sheet (England and Wales)*. HM
561 Stationery Office, London.
- 562 KEULEN, N., DEN BROK, S. & SPIERS, C. 2001. Force of crystallisation of gypsum during
563 hydration of synthetic anhydrite rock, 13th DRT conference: Deformation Mechanisms,
564 Rheology, and Tectonics.
- 565 KUSHNIR, J. 1980. The coprecipitation of strontium, magnesium, sodium, potassium and
566 chloride ions with gypsum. An experimental study. *Geochimica et Cosmochimica Acta*
567 **44**, 1471-1482.
- 568 KUSHNIR, J. 1982. The composition and origin of brines during the Messinian desiccation
569 event in the Mediterranean Basin as deduced from concentrations of ions coprecipitated
570 with gypsum and anhydrite. *Chemical Geology* **35**, 333-350.
- 571 LANDER, R. H. & LAUBACH, S. E. 2015. Insights into rates of fracture growth and sealing
572 from a model for quartz cementation in fractured sandstone. *Geological Society of*
573 *American Bulletin* **127**, 516-538.

- 574 LAUBACH, S. E., 2003. Practical approaches to identify sealed and open fractures. *AAPG*
575 *Bulletin* **87**, 561-579.
- 576 LAUBACH, S. E., REED, R. M., OLSON, J. E., LANDER, R. H. & BONELL, L. M. 2004.
577 Coevolution of crack-seal texture and fracture porosity in sedimentary rocks:
578 cathodoluminescence observations of regional fractures. *Journal of Structural Geology*
579 **26**, 967-982.
- 580 LAUBACH, S. E., OLSON, J. E. & GROSS, M. R. 2009. Mechanical and fracture stratigraphy.
581 *AAPG Bulletin* **93**, 1413-1426.
- 582 LEE, H. P., OLSON, J. E., HOLDER, J., GALE, J. F. W. & MYERS, R. D. 2015. The
583 interaction of propagating opening mode fractures with preexisting discontinuities in
584 shale. *Journal of Geophysical Research: Solid Earth* **120**, 169-181.
- 585 LESLIE, A., SPIRO, B. & TUCKER, M. 1993. Geochemical and mineralogical variations in the
586 upper Mercia Mudstone Group (Late Triassic), southwest Britain: correlation of outcrop
587 sequences with borehole geophysical logs. *Journal of the Geological Society* **150**, 67-75.
- 588 LESLIE, A. B., HARWOOD, G. M. & KENDALL, A. C. 1997. Geochemical variations within a
589 laminated evaporite deposit: evidence for brine composition during formation of the
590 Permian Castile Formation, Texas and New Mexico, USA. *Sedimentary Geology* **110**,
591 223-235.
- 592 LU, F. H., MEYERS, W. J. & SCHOONEN, M. A. 1997. Minor and trace
593 element analyses on gypsum: an experimental study. *Chemical geology* **142**, 1-10.
- 594 LU, F. H., MEYERS, W. J. & HANSON, G. N. 2002. Trace elements and environmental
595 significance of Messinian gypsum deposits, the Nijar Basin, southeastern Spain.
Chemical geology **192**, 149-161.

- 596 MACHEL, H. G. 1985. Fibrous gypsum and fibrous anhydrite in veins. *Sedimentology* **32**, 443-
597 454.
- 598 MANDL, G. 2005. *Rock joints*. Springer, Berlin.
- 599 MCINTIRE, W. L. 1963. Trace element partition coefficients - a review of theory and
600 applications to geology. *Geochimica et Cosmochimica Acta* **27**, 1209-1264.
- 601 MOHAMED EL TABAKH, B. & WARREN, J. K. 1998. Origin of fibrous gypsum in the
602 Newark rift basin, eastern North America. *Journal of Sedimentary Research* **68**, 88-99.
- 603 MURRAY, R. 1964. Origin and diagenesis of gypsum and anhydrite. *Journal of Sedimentary*
604 *Research* **34**, 512-523.
- 605 OGATA, K., SENGER, K., BRAATHEN, A. & TVERANGER, J. 2014. Fracture corridors as
606 seal-bypass systems in siliciclastic reservoir-cap rock successions: Field-based insights
607 from the Jurassic Entrada Formation (SE Utah, USA). *Journal of Structural Geology* **66**,
608 162-187.
- 609 OLD, R. 1991. *Geology of the country around Redditch*. Bernan Press (PA).
- 610 OLIVER, N. H. & BONS, P. D. 2001. Mechanisms of fluid flow and fluid-rock interaction in
611 fossil metamorphic hydrothermal systems inferred from vein-wallrock patterns,
612 geometry and microstructure. *Geofluids* **1**, 137-162.
- 613 PHILIPP, S. L. 2008. Geometry and formation of gypsum veins in mudstones at Watchet,
614 Somerset, SW England. *Geological Magazine* **145**, 831-844.
- 615 PHILLIPS, W. J. 1972. Hydraulic fracturing and mineralization. *Journal of the Geological*
616 *Society* **128**, 337-359.

- PLAYA, E., ORTI, F. & ROSELL, L. 2000. Marine to non-marine sedimentation in the upper Miocene evaporites of the Eastern Betics, SE Spain: sedimentological and geochemical evidence. *Sedimentary Geology* **133**, 135-166.
- PUTNIS, A., PRIETO, M. & FERNANDEZ-DIAZ, L. 1995. Fluid supersaturation and crystallization in porous media. *Geological Magazine* **132**, 1-13.
- ROSELL, L., ORTI, F., KASPRZYK, A., PLAYA, E. & PERYT, T.M. 1998. Strontium geochemistry of Miocene primary gypsum: Messinian of southeastern Spain and Sicily and Badenian of Poland. 1998. *Journal of Sedimentary Research* **68**, 63-79.
- RUFFEL, A. 1990. Stratigraphy and structure of the Mercia Mudstone Group (Triassic) in the western part of the Wessex Basin. *Proceedings of the Ussher Society* **7**, 263-267.
- RUFFEL, A. 1991. Palaeoenvironmental analysis of the late Triassic succession in the Wessex Basin and correlation with surrounding areas. *Proceedings of the Ussher Society* **7**, 402-407.
- RUSTICHELLI, A., DI CELMA, C., TONDI, E., BAUD, P. & VINCIGUERRA, S. 2016. Fibrous gypsum veins as diffuse features and within fault zones: the case study of the Pisco Basin (Ica desert, southern Peru). *Journal of the Geological Society* **173**, 405-418.
- SEEDHOUSE, J. & RACEY, A. 1997. Sealing capacity of the Mercia Mudstone Group in the East Irish Sea Basin: implications for petroleum exploration. *Journal of Petroleum Geology* **20**, 261-286.
- SELLWOOD, B. & SLADEN, C. 1981. Mesozoic and Tertiary argillaceous units: distribution and composition. *Quarterly Journal of Engineering Geology and Hydrogeology* **14**, 263-275.

- 639 SHEARMAN, D., MOSSOP, G., DUNSMORE, H. & MARTIN, M. 1972. Origin of gypsum
640 veins by hydraulic fracture. *Institution of Mining and Metallurgy Transaction, Section B:*
641 *Applied Earth Science* **81**, 149-155.
- 642 SMITH, E. G., RHYS, G. H. & GOOSSENS, R. 1974. *Geology of the country around East*
643 *Retford, Worksop and Gainsborough*. British Geological Survey, Keyworth.
- 644 TALBOT, M., HOIM, K. & WILLIAMS, M. 1994. Sedimentation in low-gradient desert margin
645 systems: A comparison of the Late Triassic of northwest Somerset (England) and the
646 late Quaternary of east-central Australia. *Geological Society of America Special Papers*
647 **289**, 97-117.
- 648 TAYLOR, S. 1983. A stable isotope study of the Mercia Mudstones (Keuper Marl) and
649 associated sulphate horizons in the English Midlands. *Sedimentology* **30**, 11-31.
- 650 TRUDE, J., GRAHAM, R. & PILCHER, R. 2012. Salt-related structures on the Bristol Channel
651 coast, Somerset (UK). *Geological Society, London, Special Publications* **363**, 533-544.
- 652 TUCKER, M. 1977. The marginal Triassic deposits of South Wales: continental facies and
653 palaeogeography. *Geological Journal* **12**, 169-188.
- 654 TUCKER, M. E. 1978. Triassic Lacustrine Sediments from South Wales: Shore□Zone,
655 Evaporites and Carbonates. In: Matter, A., Tucker, M.E. (Eds.) *Modern and Ancient*
656 *Lake Sediments*, 205-224.
- 657 WARRINGTON, G. 1974. Studies in the palynological biostratigraphy of the British Trias. I.
658 Reference sections in west Lancashire and north Somerset. *Review of Palaeobotany and*
659 *Palynology* **17**, 133-147.
- 660 WARRINGTON, G. 1980. *A correlation of Triassic rocks in the British Isles*. Blackwell
661 Scientific.

- 662 WARRINGTON, G. & IVIMEY-COOKC, H. 1992. Triassic. 97-106 in Atlas of
663 palaeogeography and lithofacies. *Geological Society of London Memoir* **13**.
664 WHITTAKER, A. & GREEN, G. W. 1983. *Geology of the country around Weston-super-Mare*.
665 Memoirs of the Geological Survey of Great Britain. HM Stationery Office, London.
666 WILLIAMS, J., HOLLOWAY, S. & WILLIAMS, G. 2014. Pressure constraints on the CO₂
667 storage capacity of the saline water-bearing parts of the Bunter Sandstone Formation in
668 the UK Southern North Sea. *Petroleum Geoscience* **20**, 155-167.
669 WILSON, A. 1990. The Mercia Mudstone Group (Trias) of the East Irish Sea Basin.
670 *Proceedings of the Yorkshire Geological and Polytechnic Society* **48**, 1-22.
671 WILSON, A. 1993. The Mercia Mudstone Group (Trias) of the Cheshire Basin. *Proceedings of*
672 *the Yorkshire Geological and Polytechnic Society* **49**, 171-188.
673 WILTSCHKO, D. V. & MORSE, J. W. 2001. Crystallization pressure versus “crack seal” as the
674 mechanism for banded veins. *Geology* **29**, 79-82.

1
2
3
4
5
6
7
8
9
10
11
12
13
14
15
16
17
18
19
20
21
22
23
24
25
26
27
28
29
30
31
32
33
34
35
36
37
38
39
40
41
42
43
44
45
46
47
48
49
50
51
52
53
54
55
56
57
58
59
60

685 Table 1 Data for gypsum cement and gypsum vein content (vol. %) in the host rock from non-
686 nodular beds.

Host rock	Content	
	Vein	Cement
Sandstone, Unit 1	14.2	12.5
Marl, Unit 1	7.1	8.7
Silty Marl, Unit 2	25.4	28.2
Calcareous marl, Unit 3	0	0
Marl, Unit 4	9.5	10.3
Marl, Unit 5	0	0

687

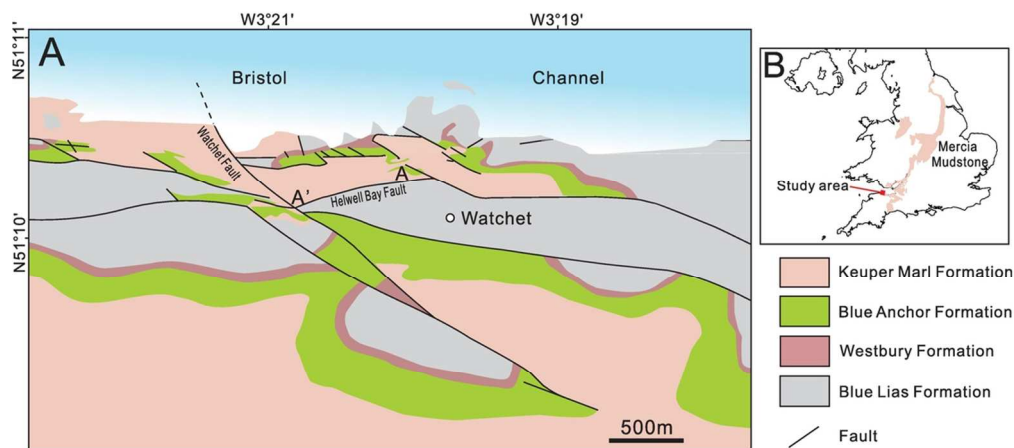
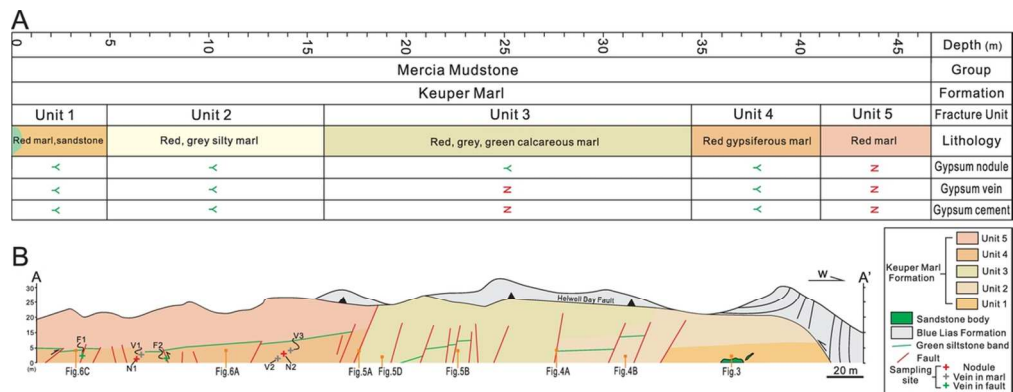


Figure 1. Geological map of the Watchet area (A) and outcrop distribution of the Mercia Mudstone in the UK (B). Modified from Glen et al. (2005) and Howard et al. (2008).

102x58mm (300 x 300 DPI)



103x39mm (300 x 300 DPI)

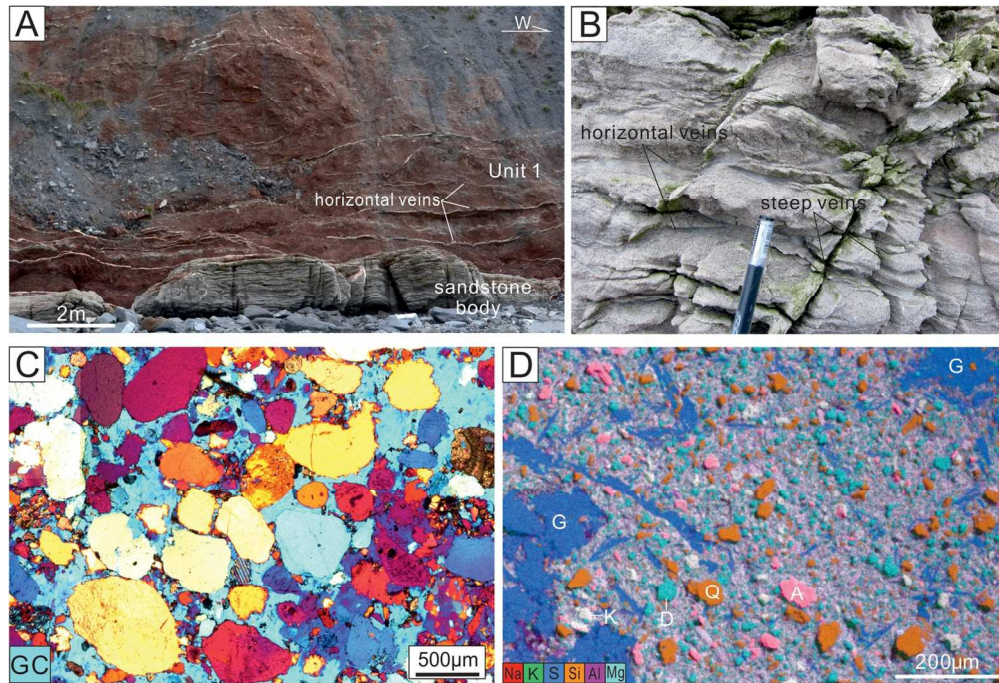


Figure 3. (A) Outcrop photograph showing the sandstone base and red marls of Unit 1. Note the white bands of horizontal gypsum veins. (B) Dense gypsum veins in the sandstone body. (C) Photomicrograph showing the gypsum cement of the sandstone. GC, gypsum cement. Crossed polars, with gypsum plate inserted. (D) EDS image showing fabric and mineral composition of the marl from Unit 1. A, albite. D, dolomite. G, gypsum. K, K-feldspar. Q, quartz.

137x93mm (300 x 300 DPI)

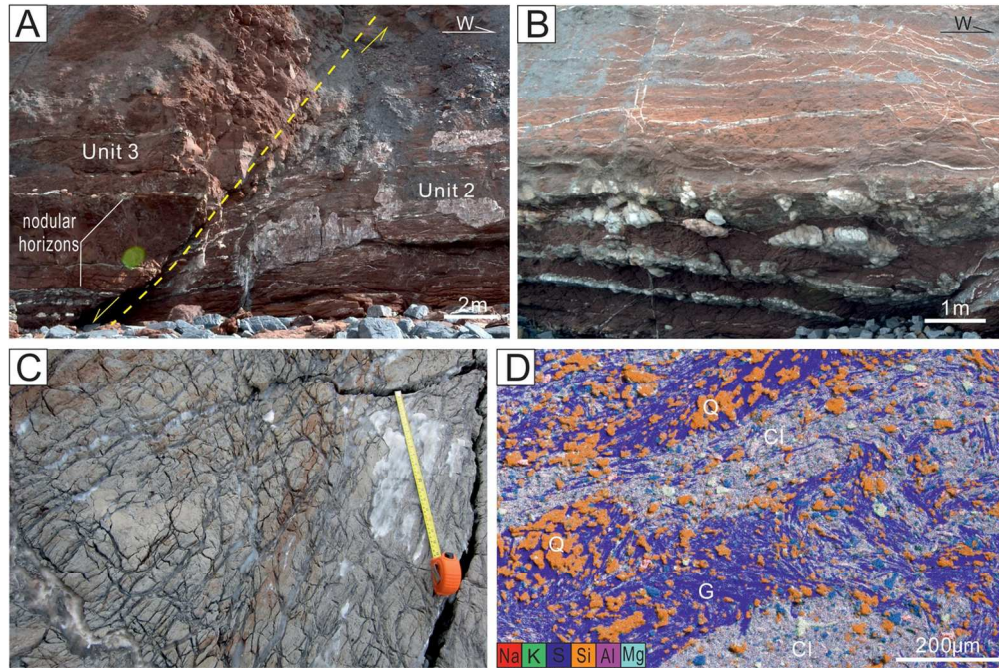


Figure 4. (A) Outcrop photograph showing Unit 2 in the footwall of a normal fault, and Unit 3 in the hanging wall of the fault. Note that gypsum veins are rare in Unit 3, whereas veins are intensively developed in Unit 2. (B) Dense gypsum veins in red marls above nodular gypsum horizons. (C) Highly fractured grey siltstone in Unit 2. All fractures are filled with gypsum. Tape measure is 50 cm. (D) EDS image showing fabric and mineral composition of the silty marl from Unit 2. Cl, clay. G, gypsum. Q, quartz.

126x83mm (300 x 300 DPI)

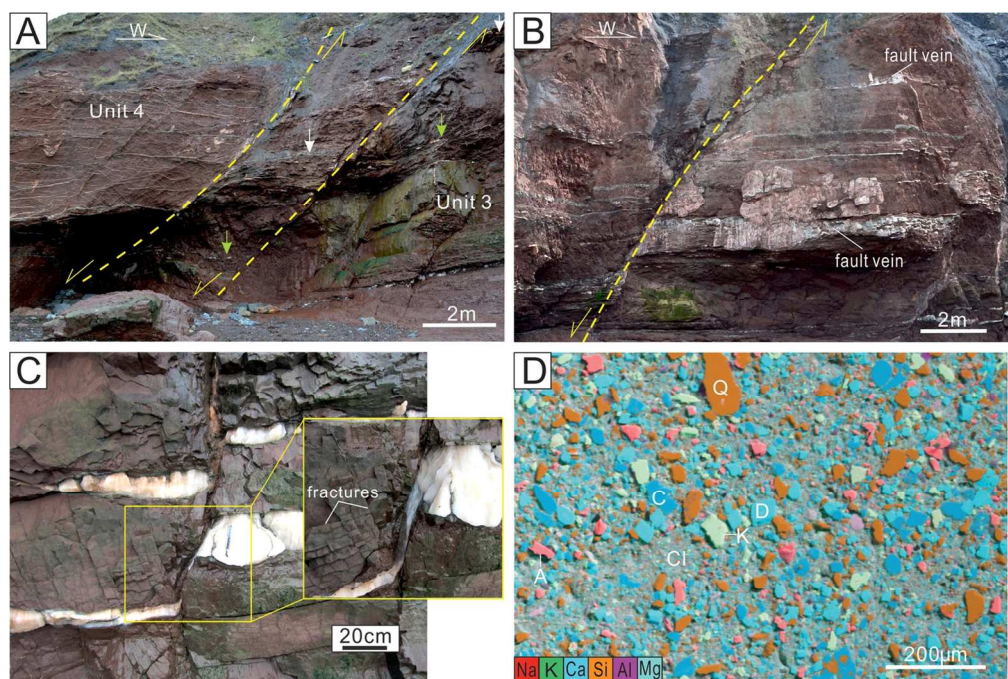


Figure 5. (A) Outcrop photograph showing Unit 3 in the footwall of a normal fault, and Unit 4 in the hanging wall of another normal fault. Note the different levels in vein abundance between Unit 4 and Unit 3. Arrows mark the horizons that can be correlated. (B) Normal faults partially filled with gypsum in Unit 3. Note that white gypsum fills mainly occur in the segment adjacent to nodular gypsum horizons. (C) Close view of a nodular gypsum horizon. Note the open fractures without gypsum cementation. (D) EDS image showing fabric and mineral composition of the marl from Unit 3. A, albite. C, calcite. Cl, clay. D, dolomite. K, K-feldspar.

130x87mm (300 x 300 DPI)

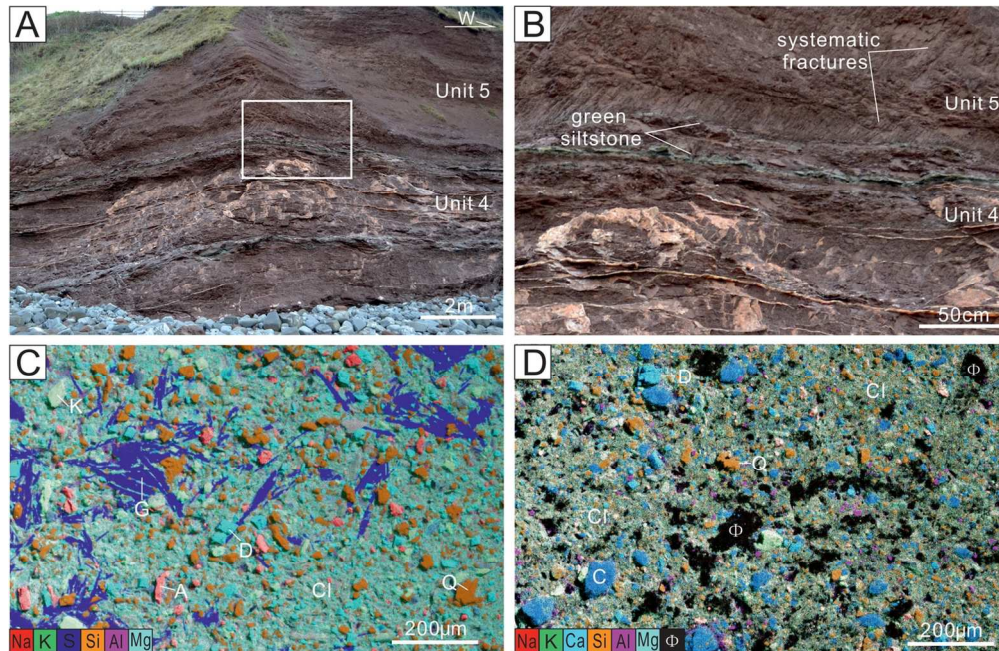


Figure 6. (A) Outcrop photograph showing Units 4 and 5. Note the absence of veins in Unit 5, and the dense gypsum veins in Unit 4. (B) Close view of the boundary between Unit 4 and Unit 5. Note the parallel, systematic fractures in Unit 5, which are parallel to the steep veins in Unit 4, but not filled with gypsum. See location in the box of Figure 6A. (E) and (F) EDS image showing fabric and mineral composition of marl from Unit 4 and Unit 5 respectively. A, albite. C, calcite. Cl, clay. D, dolomite. G, gypsum. Φ , pore space.

128x83mm (300 x 300 DPI)

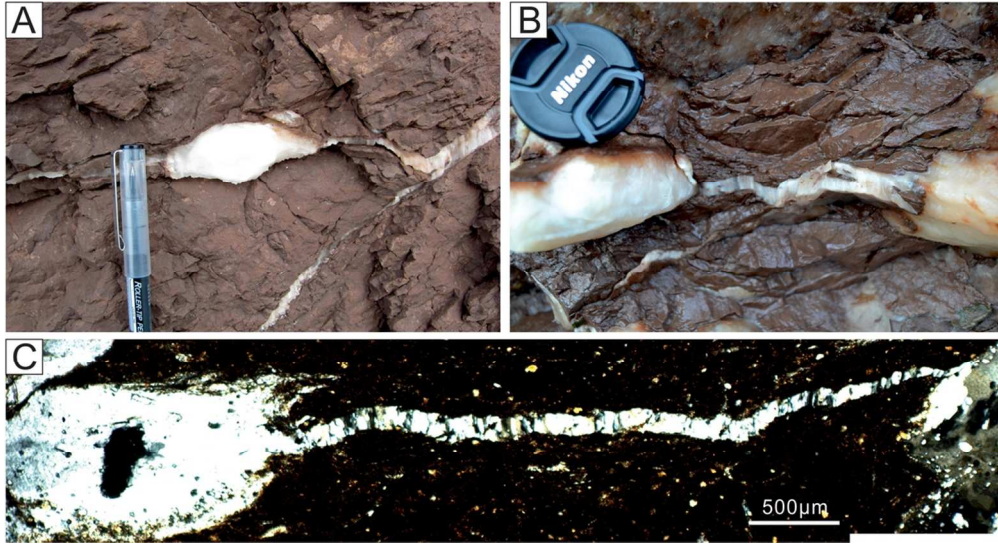


Figure 7. Nodule-rooted horizontal gypsum veins in red marls. (A) Gypsum veins on both the left and right sides of a homogeneous gypsum nodule. (B) A horizontal gypsum vein linking two neighboring nodules. (C) Photomicrograph showing a gypsum vein linking two nodules. The vein is interpreted to be rooted in the left nodule and have propagated towards the right nodule, based on the decreased aperture. Crossed polars.

105x56mm (300 x 300 DPI)

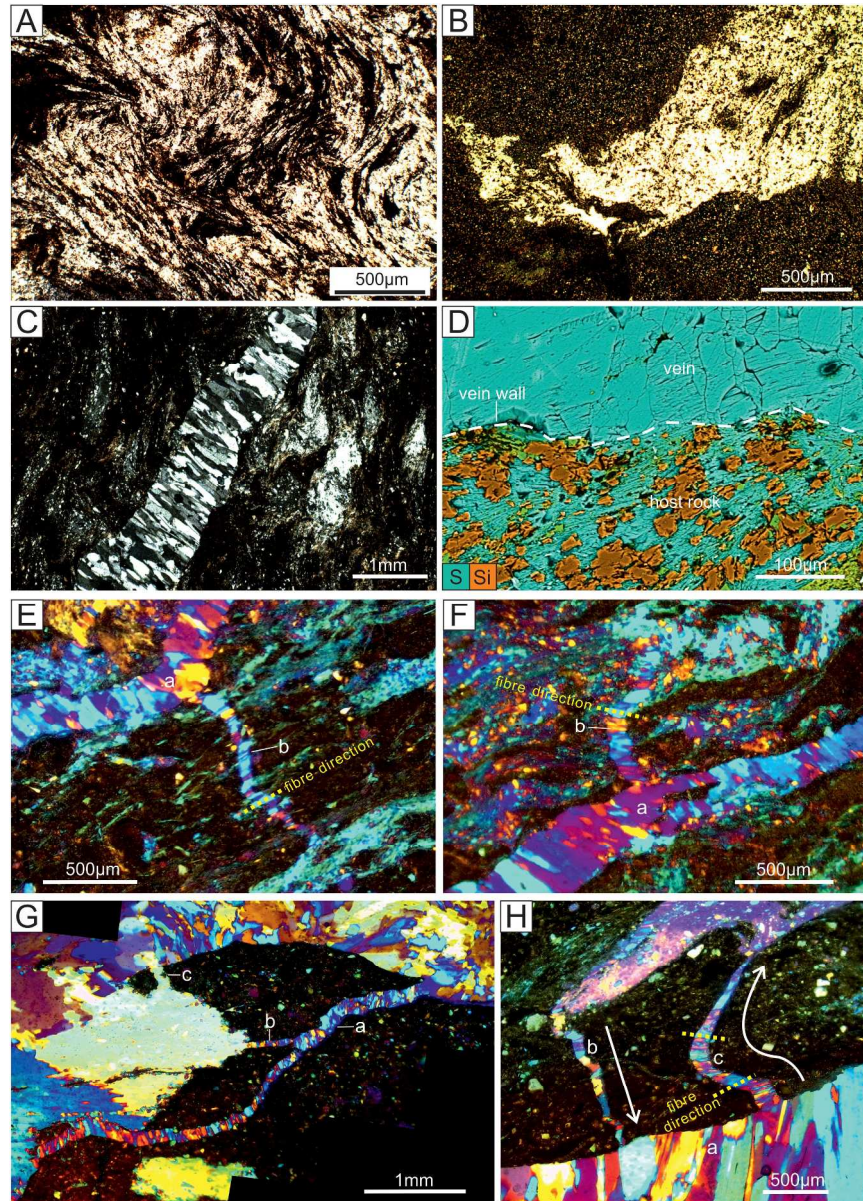


Figure 8. Photomicrographs showing gypsum in the host rock. (A) Dense gypsum laths exhibiting a flowing appearance. (B) Diffusely disseminated gypsum in siltstone. Crossed polars. (C) Structureless poikilotopic gypsum cement near a fibrous gypsum vein. (D) EDS image showing widely disseminated gypsum in the wall rock of a gypsum vein. The dashed line marks the vein boundary. (E) A minor gypsum vein b linking vein a and blocky gypsum masses in clay-rich marl. (F) Vein b linking vein a and blocky gypsum cements in silty marl. (G) Vein a, b and c linking gypsum masses, leading to the segmentation of the host rock. Note that both ends of vein a and c are rooted in the gypsum masses. (H) Two minor veins (b and c) linking a large gypsum vein a with a blocky gypsum body. The arrows mark the propagation direction of the minor veins, indicated by the decreased aperture of the veins. The dashed lines mark fibre directions. Crossed polars, with gypsum plate inserted (8E-H).

230x322mm (300 x 300 DPI)

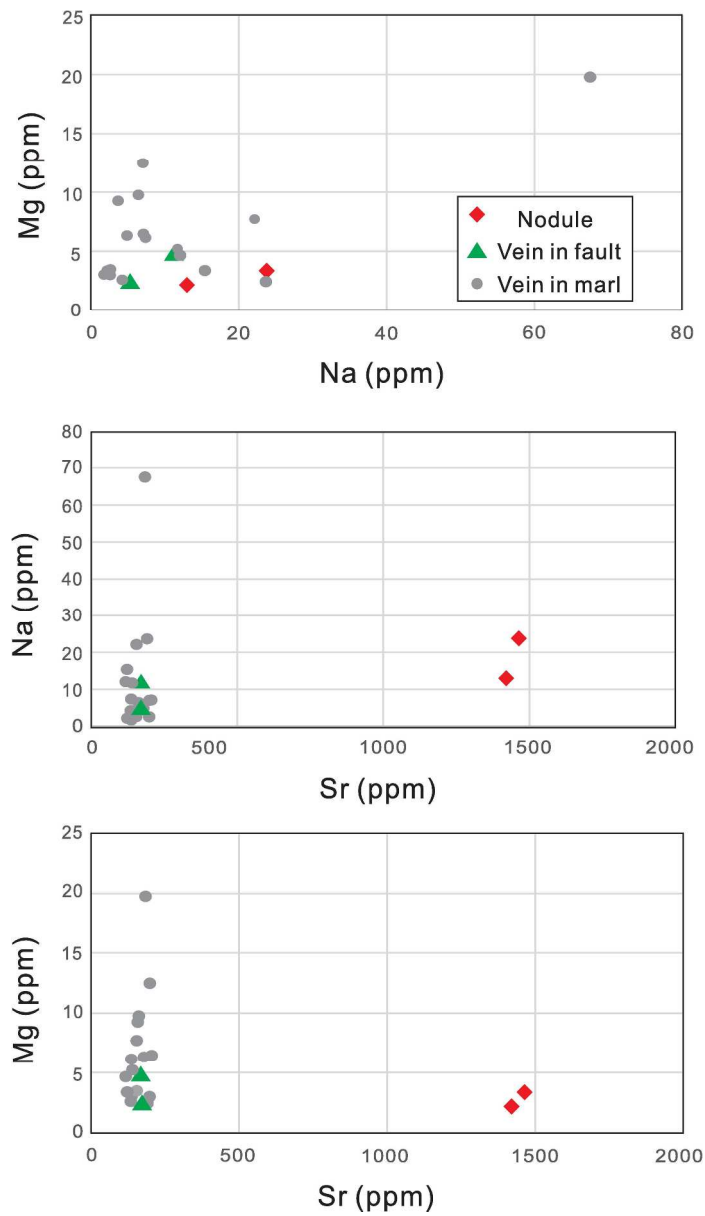


Figure 9. Elemental concentration plot of Na vs. Mg, Sr vs. Na, Sr vs. Mg from samples of gypsum nodules, gypsum veins in marls and gypsum veins in faults. See sample locations in Figure 2B.

211x367mm (300 x 300 DPI)

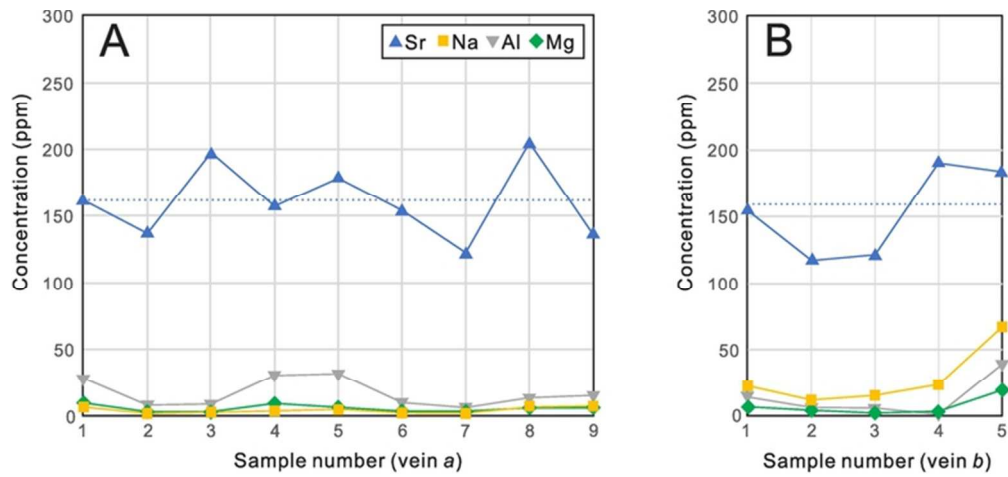


Figure 10. Elemental concentration plot of Sr, Na, Al and Mg from gypsum vein a (A) and vein b (B). The dashed line mark the average value of Sr concentration.

65x30mm (300 x 300 DPI)

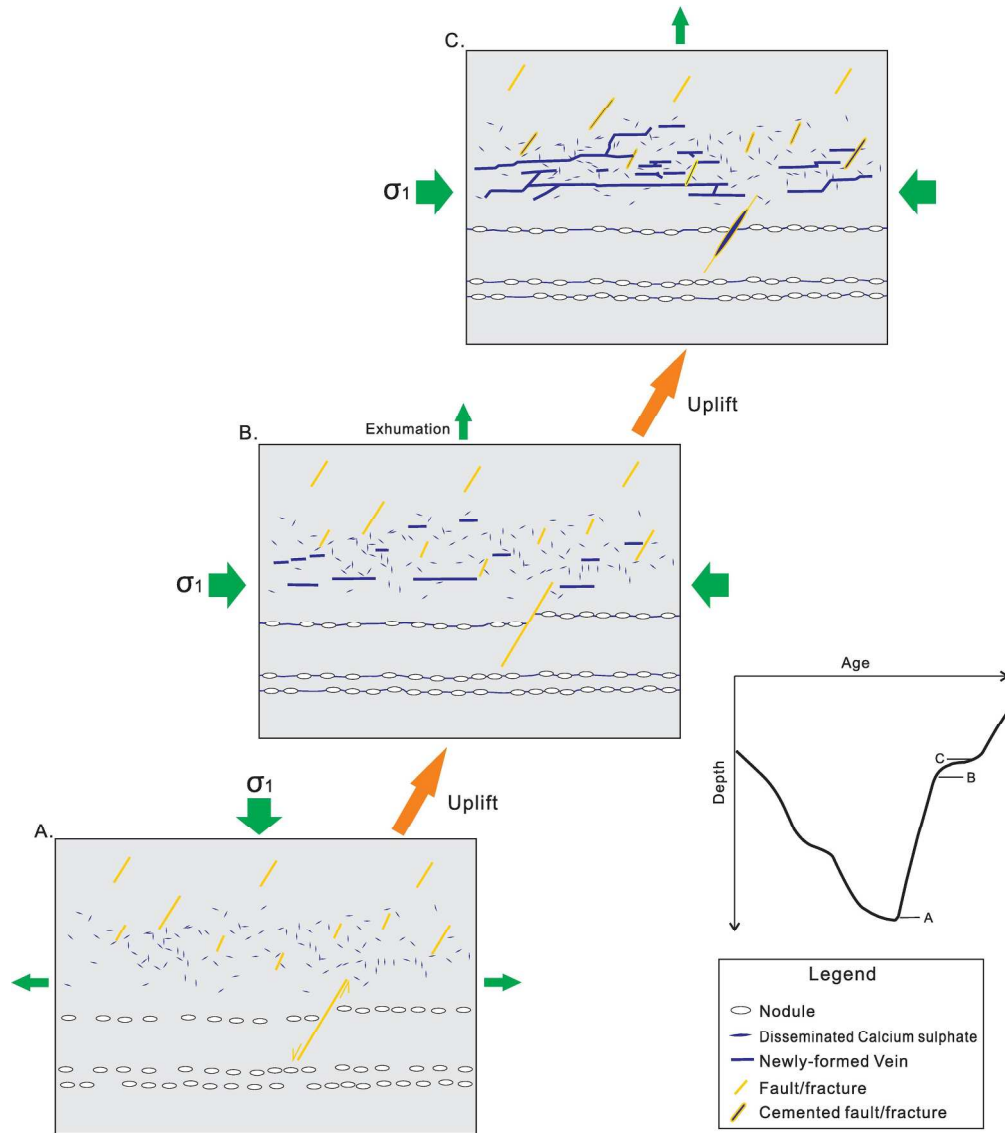


Figure 11. Sketch illustrating the diagenetic processes of calcium sulphate during uplift of the Keuper Marl. (A) Burial anhydrite in the form of discrete laths and nodules at the maximum depth. (B) Onset of anhydrite hydration during uplift of the marl. Note the formation of nodule-rooted veins. (C) Precipitation of gypsum in both the pre-existing fractures and newly-formed hydraulic fractures. Gypsum is transported to adjacent veins mainly through diffusion after fracture initial propagation. Note that fractures in gypsum-free rocks are not filled. The burial curve is modified from Cosgrove (2001).

221x249mm (300 x 300 DPI)

Geological Magazine

Lithological control on fracture cementation in the Keuper Marl (Triassic), north Somerset, UK

Qingfeng Meng, John Hooker & Joe Cartwright

Supplementary Material

Table S1 Elemental concentrations (ppm) of gypsum nodules, fault veins and veins from red marls. See sample locations in Fig. 2B.

	Nodule 1	Nodule 2	Fault vein 1	Fault vein 2	Vein 1									Vein 2					Vein 3		
					1	2	3	4	5	6	7	8	9	1	2	3	4	5	1	2	3
Al	2.074	0.480	6.595	8.687	27.938	7.702	8.841	30.369	31.718	9.801	6.041	12.708	15.069	13.939	5.869	5.376	0.095	39.692	6.551	4.441	
Ba	7.139	0.204	0.324	0.363	0.747	0.200	0.152	0.518	0.849	0.389	0.590	0.751	0.189	0.233	0.142	0.192	0.011	0.716	0.079	0.104	0.551
Cr	0.034	0.591	9.206	0.668	0.248	0.443	0.901	1.707	0.999	1.339	8.509	1.403	1.205	1.201	0.595		0.650	0.663	0.353	0.059	0.364
Cu	0.511	1.263	5.263	0.098	0.418	0.228	0.202	0.125	0.293	0.232	1.740	5.944	0.237	0.113	0.067	0.633	0.079	0.219	0.093	0.425	0.127
Fe	24.680	36.513	31.277	24.665	28.609	23.464	32.877	25.750	28.093	25.840	20.973	34.479	21.915	32.807	22.897	22.068	32.608	30.643	28.007	24.095	34.722
Mg	3.358	2.154	4.788	2.295	9.754	3.036	3.007	9.257	6.335	3.488	3.378	6.464	6.1484	7.721	4.665	3.374	2.445	19.769	5.235	2.607	12.465
Mn	0.832	0.402	5.403	0.079	1.579	0.956	1.332	0.608	0.585	1.298	16.951	17.000	1.142	0.205		1.186	0.044	0.506	0.109	1.615	0.378
Na	23.768	12.977	11.455	5.229	6.415	1.736	2.548	3.606	4.877	2.583	2.144	7.093	7.368	22.106	12.059	15.404	23.655	67.503	11.699	4.197	7.019
Ni	7.929	9.008	13.829	5.811	6.910	7.582	8.732	6.566	4.654	6.419	10.416	12.234	7.565	10.972	8.350	10.113	6.313	5.319	5.380	6.830	7.936
Pb	0.074	0.062	0.236		1.148	0.072	0.392	0.095	0.159	0.178	1.003	0.484	0.047	0.019	0.015	0.046		0.132		0.047	0.140
Rb	0.167	0.052	0.393	0.397	1.471	0.414	0.320	1.368	2.218	0.796	0.402	0.407	0.445	0.405	0.323	0.319	0.055	1.719	0.308	0.345	1.115
Ru	0.360	0.268	0.055	0.028	0.024	0.032	0.028	0.023	0.029	0.026	0.039	0.032	0.029	0.022	0.029	0.042	0.023	0.022	0.021	0.052	0.031
Sr	1463.544	1420.214	170.037	171.733	161.398	136.872	197.549	157.151	178.293	153.943	122.527	204.913	136.060	154.269	117.057	121.683	190.481	183.623	139.137	134.482	198.659
Ti		0.042	0.165	0.025	0.364	0.128	0.093	0.162	0.284	0.049	0.016	1.365	0.063	0.166	0.015	0.007		0.290	0.031	0.005	0.164
Th			0.057	0.021	0.242	0.075	0.012	0.316	0.186	0.039	0.077	0.246	0.052	0.078	0.077	0.077		0.148	0.012	0.444	0.114
U	0.005		0.051	0.012	0.142	0.014	0.009	0.063	0.141	0.022	0.080	0.020	0.014	0.026	0.008	0.015		0.083	0.006	0.054	0.047
V	0.908	0.532	1.147	0.439	1.399	0.582	0.648	0.933	1.910	0.682	1.481	0.974	0.649	0.574	0.491	1.191	0.340	1.405	0.366	0.402	1.017
Zn	5.179	2.333	3.532	2.086	1.561	1.821	2.291	1.795	5.238	3.878	2.704	5.857	1.896	1.823	1.930	2.625	1.836	2.807	1.468	2.594	4.084
Zr			0.537	0.113	2.558	0.156	0.174	1.119	0.858	1.678	1.831	0.569	0.294	0.319	0.607	0.261	0.042	0.758	0.077	0.479	1.162